Mineralium Deposita (2005) 40: 289–306
DOI 10.1007/s00126-005-0024-8

ARTICLE

Volker Lüders · Rolf L. Romer
Alexandre R. Cabral · Christian Schmidt
David A. Banks · Jens Schneider

Genesis of itabirite-hosted Au–Pd–Pt-bearing hematite-(quartz) veins, Quadrilátero Ferrífero, Minas Gerais, Brazil: constraints from fluid inclusion infrared microthermometry, bulk crush-leach analysis and U–Pb systematics

Received: 1 March 2005 / Accepted: 11 August 2005 / Published online: 7 October 2005

Abstract Fluid inclusions hosted in quartz and specular hematite from auriferous (*jacutinga*) and barren veins in the Quadrilátero Ferrífero (QF) have been studied using conventional and near infrared microscopy, respectively. The mineralization consists of veins that cross-cut metamorphosed iron formation (itabirite) of the Paleoproterozoic Itabira Group. The sample suite comprises hematite from veins from the low-strain domain in the W and SW of the study area, as well as hematite samples from the eastern high-strain domain in the central and NE parts of the QF. Halogen ratios of fluid inclusions in quartz and hematite from all studied deposits are consistent with a fluid evolved from dissolving and reprecipitating halite that was subsequently diluted. Fluid inclusions hosted in quartz and hematite are characterized by consistent Na/K ratios and considerable SO_4 contents, and suggest similar formation conditions and, perhaps, fluid origin from a common source. Na/K and Na/Li fluid mineral geothermometers indicate water–rock interaction at approximately 340 ± 40°C. Hematites from the high-strain domain contain fluid inclusion assemblages of high-temperature aqueous-carbonic and multiphase high-salinity, high-temperature aqueous inclusions probably due to fluid immiscibility in the system H_2O–NaCl–CO_2. Fluid inclusions hosted in hematite from barren veins in the low-strain domain, as well as in hematite from *jacutinga*-type mineralization from the central part of the QF, only host multiphase aqueous fluid inclusions all showing narrow ranges of salinity (7.2–11.7 wt.% NaCl equiv.) and homogenization temperatures (148 to 229°C). Lower homogenization temperatures and the absence of CO_2-rich inclusions in specular hematite from these occurrences are attributed to carbonate precipitation and/or CO_2 escape due to cooling during fluid migration from the high- to the low-strain domain. Pb–Pb and U–Pb systematics of gold, hematite and hematite-hosted fluid inclusions in combination with geochemical evidence indicate distinct sources for Pd, Au, and Pb. The formation of specular hematite veins may be related to retrograde metamorphic fluids being released during the Brazilian orogenic cycle (600–700 Ma). The Pb isotopic characteristics of all samples are readily reconciled in a simple model that involves two different Paleoproterozoic or Archean source lithologies for lead and reflects contrasting depths of fluid percolation during the Brasiliano orogeny.

Keywords Fluid inclusions · Infrared microscopy · U–Pb · *Jacutinga* veins · Au–Pd–Pt · Minas Gerais

Editorial handling: B. Lehmann

V. Lüders (✉) · R. L. Romer · C. Schmidt
GeoForschungsZentrum Potsdam, Telegrafenberg,
14473 Potsdam, Germany
E-mail: volue@gfz-potsdam.de

A. R. Cabral
Institut für Mineralogie und Mineralische Rohstoffe,
Technische Universität Clausthal, Adolph-Roemer-Strasse 2A,
38678 Clausthal-Zellerfeld, Germany

D. A. Banks
School of Earth Sciences, University of Leeds, Leeds, LS2 9JT, UK

J. Schneider
Institut für Geowissenschaften und Lithosphärenforschung,
Justus-Liebig-Universität Gießen, Senckenbergstrasse 3,
35390 Giesen, Germany

Present address: A. R. Cabral
Département de géologie et de génie géologique,
Université Laval, Pavillon Adrien-Pouliot,
Québec, QC G1K 7P4, Canada

Introduction

Palladian gold mineralization is rare and occurrences of economic importance seem to be known from Brazil

only. During the Brazilian Gold Cycle (1695–1785), much of the gold production from the area around the city of Ouro Preto (Minas Gerais) presumably came from palladian gold mineralization hosted by banded iron formations, i.e. *itabirites* (e.g. Scott 1902). A recent gold rush (1980–1984) at Serra Pelada in the Carajás mineral province, northern Brazil, focused again on this type of mineralization (e.g. Meireles and Silva 1988; Cabral et al. 2002a).

In the Quadrilátero Ferrífero (QF) of Minas Gerais (Fig. 1), the auriferous portions of itabirites have traditionally been denoted as *jacutinga* (Hartt 1870; Hussak 1904). This peculiar mineralization occurs as Au–Pd–Pt-bearing quartz-specular hematite veins (Fig. 2a–d) cross-cutting the metamorphosed host itabirites (e.g. H.F. Galbiatti, unpublished Msc Thesis). The gold is coarse-grained and commonly black (*ouro preto*) due to coatings of Pd–O and oxyhydroxide (Johnson and Lampadius 1837; Jedwab and Cassedanne 1998; Cabral et al. 2001, 2003a). A number of *jacutinga*-style gold deposits were worked in the eighteenth and nineteenth centuries in the Quadrilátero Ferrífero. The most famous one was Gongo Soco (Fig. 1), the first major underground mine in Brazil, with a total production of 12.9 metric tons Au between 1826 and 1856 (Henwood 1871). Its spectacular gold-rich "bunches", from which Hart in May 1827 "brought out of the mine, in a miner's hat, eleven pounds of gold" (Hart 1827), motivated copious reports by early workers, as documented by Henwood (1871). The first chemical investigations date back to 1826, when palladium was identified (Gardner 1826). The old underground workings collapsed and were flooded after gold mining ceased in 1857, and thus became inaccessible. Only recently, iron ore opencast mining operations have exposed sections of *jacutinga* mineralization. Gold is currently an intermittent by-product of iron ore mining at Gongo Soco (several tens of kilogram Au per year) and Itabira (Fig. 1), where gold production amounted to about 600 kg Au per year in 2000, but has now decreased due to closure of one of the important mines (Cauê) in 2004.

The genesis of *jacutinga*-style gold mineralization is enigmatic and has long been debated (Hussak 1904; Oliveira 1932; Guimarães 1970). Recently, Olivo et al. (1995, 1996, 2001) have claimed that the mineralization is structurally controlled, i.e. running parallel to the mylonitic foliation, and formed ca. 1.83 Ma ago at about 600°C during Transamazonian peak metamorphism. We utilize near infrared microscopy on hematite-hosted fluid inclusions (Lüders et al. 1999), bulk crush-leach analysis (Banks et al. 2000), and U–Pb isotope systematics in order to place constraints on the origin, formational conditions and age of itabirite-hosted *jacutinga*-style Au–Pd–Pt vein mineralization at Gongo Soco and Itabira (Fig. 1). For comparison, specular hematite-rich veins barren of palladian gold from the Córego do Feijão and Fábrica iron ore deposits, situated in the low-strain domain of the Quadrilátero Ferrífero (Fig. 1), have also been studied.

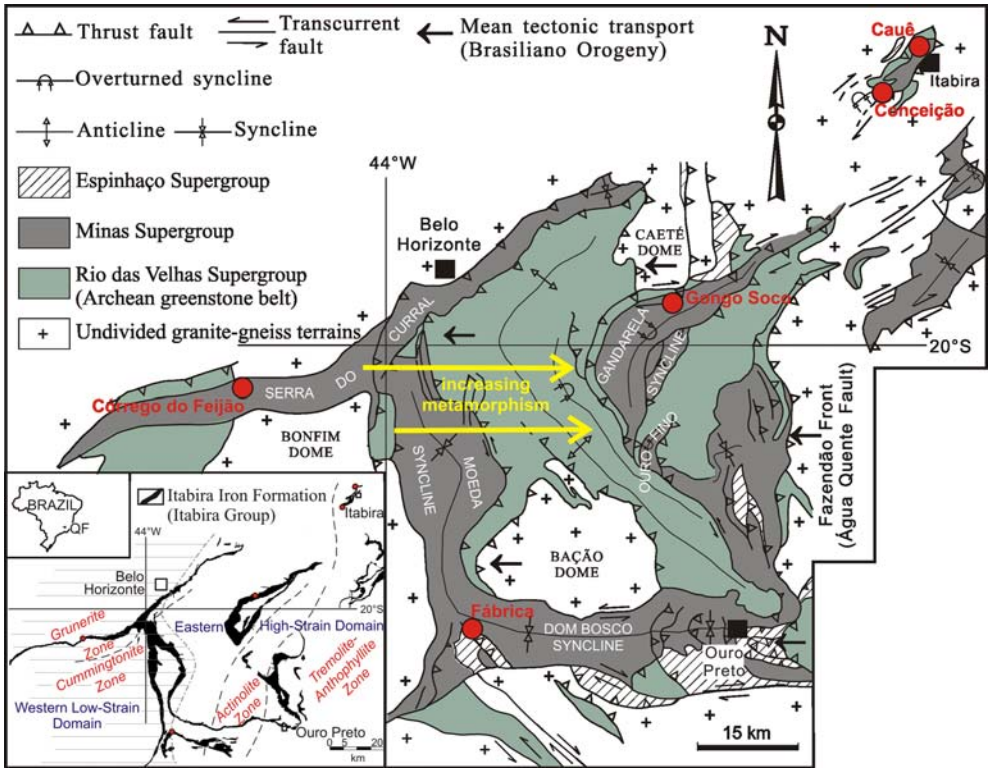

Fig. 1 Simplified geological map of the Quadrilátero Ferrífero (modified after Rosière et al. 2001). *Inset*: metamorphic zones (*dashed lines*, Pires 1995) and strain domains (Rosière et al. 2001) in the Itabira iron formation (Itabira Group)

Geology and mineralization

Regional geology

The QF of Minas Gerais (Fig. 1) consists of a Paleoproterozoic clastic-chemical sedimentary sequence (Minas Supergroup) underlain by an Archean greenstone belt (Rio das Velhas Supergroup) surrounded by granite-gneiss terrains. Important iron ore deposits and subordinate deposits of bauxite and manganese oxide are hosted by the Itabira iron formation sensu Harder and Chamberlin (1915), later designated as the Itabira Group (Dorr 1969). The Itabira Group comprises a continuous sequence of Paleoproterozoic chemical sedimentary rocks subdivided into two formations, (1) the Cauê Formation, a thick iron formation (itabirite) which grades upwards into dolomitic rocks of the (2) Gandarela Formation. The Itabira Group defines the intermediate chemical sedimentary succession of the Minas Supergroup, overlying the basal Caraça Group. The Caraça Group is divided into two formations: (1) the subjacent Moeda Formation which consists of quartzites, uraniferous and auriferous metaconglomerates and sericite schists; and (2) the superjacent Batatal Formation which is composed of phyllites, boron-bearing schists and mafic greenstones (Pires 1983). It also contains carbonaceous phyllites with occasional pyrite nodules of organic origin, similar to the Mount McRae Shale of the Hamersley Province, Australia (C.A. Rosière, personal communication). The Itabira Group is overlain by the Piracicaba Group which is characterized by quarzites and phyllites containing minor iron formations. The Minas Supergroup rests unconformably on the Archean Rio das Velhas Supergroup, a greenstone sequence (Lobato et al. 2001 and references therein). The regional structures of these sedimentary belts have been considered to be the result of two main tectonic events (e.g. Chemale et al. 1994; Alkmim and Marshak 1998), The first event is the 2.1–2.0 Ga Transamazonian orogeny, represented by two sets of structures: (1) NW-vergent folds and thrusts affecting the Rio das Velhas Supergroup and the Minas Supergroup (collisions stage), (2) followed by structures developed as a consequence of emplacement of basement domes (collapse stage) (Alkmim and Marshak 1988). The second event is the 0.7–0.6 Ga Pan-African-Brasiliano orogeny, a W-verging fold-and-thrust belt. The Pan-African-Brasiliano compressive tectonics produced pervasive tectonic fabrics in the region east of the Moeda Syncline (Fig. 1). These fabrics include penetrative mylonitic foliation (S_1) and ESE-plunging stretching lineation, as well as mesoscopic folds with E-W-trending axes and late N–S-trending

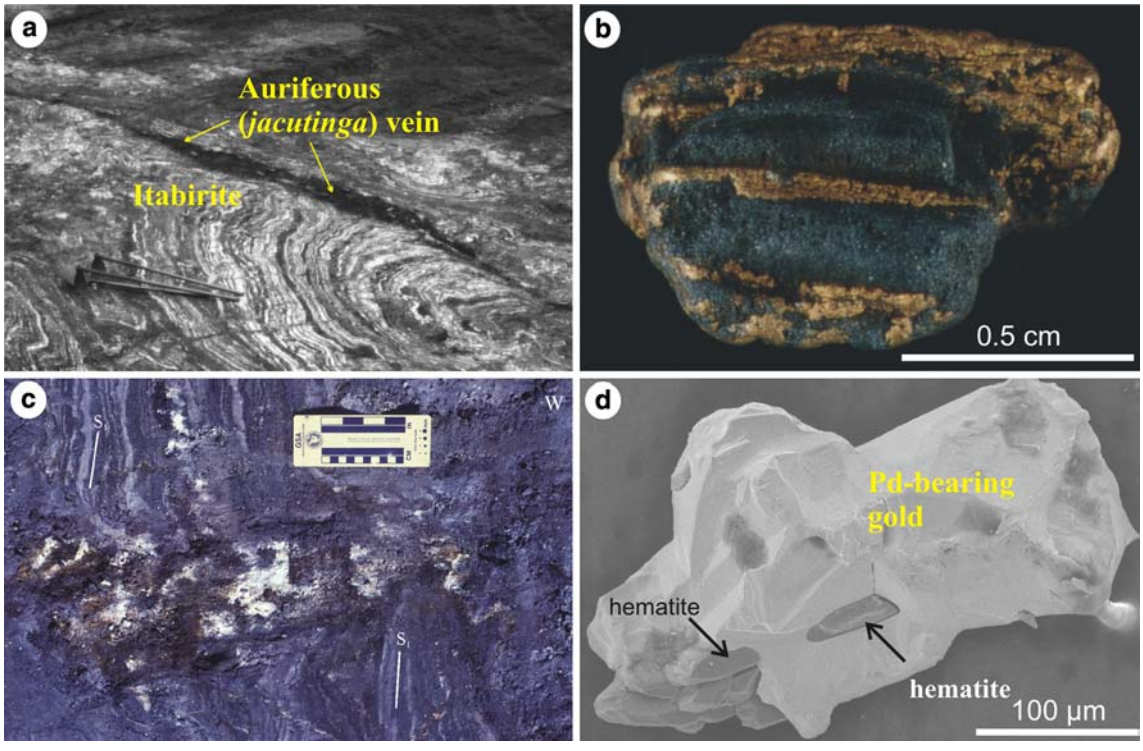

Fig. 2 **a** Specular hematite-rich auriferous vein (*jacutinga*) truncates folded itabirite at Gongo Soco. The itabirite banding is defined by quartz (*white*) and hematite (*dark*). The vein (dark stripe) approximately runs from east (left end of the vein) to west (right end). The hoes are about 1.5 m long. **b** Auriferous aggregate recovered from a Knelson concentrator at the Gongo Soco iron ore plant. Palladiferous gold crosscuts the main foliation (S_1) given by fine-grained hematite (*dark*). **c** *Jacutinga* vein, of quartz (*white*) and specular hematite (*dark*), perpendicularly transects the S_1 foliation of the host itabirite at Cauê, Itabira (Central orebody, level 740). **d** Secondary electron image of palladiferous gold with inclusions of hematite from a *jacutinga* vein, Cauê, Itabira (Y orebody, level 725)

crenulation lineation (e.g., Chemale et al. 1994; Alkmim and Marshak 1998). The metasedimentary rocks of the QF display a regional metamorphic zoning with greenschist-facies conditions in its western and central parts increasing to almandine-amphibolite facies in the eastern part (Pires 1995 and references therein). Pires (1995) defined metamorphic zones for the Itabira Group as follows: the *grunerite* and *cummingtonite zones*, respectively, occupy the western and central parts of the QF, whereas the *actinolite* and *tremolite-anthophyllite zones* prevail in its eastern part (Fig. 1).

Au–Pd–Pt-bearing (jacutinga-style) and barren hematite vein mineralization in the QF

Jacutinga is a sulfide-free palladiferous gold-bearing mineralization consisting of soft and specular hematite with variable amounts of quartz and subordinate kaolinite, talc, goethite and manganese oxides (Hussak 1904). The *jacutinga* mineralization occurs as generally narrow (a few centimeter wide) veins crosscutting metamorphosed host itabirites (Fig. 2a, c). Gold occurs as free and visible granules (Fig. 2b), flakes and threads in the soft *jacutinga* (Fig. 2d), but not in hard hematite ore (Henwood 1871). The mineralization has a minor, but significant Sb–As–Se-Hg component, as reflected by the presence of Pd- and Pt-bearing selenides and arsenoantimonides of palladium (e.g. Clark et al. 1974; Davis et al. 1977; Olivo and Gauthier 1995; Kwitko et al. 2002; Cabral et al. 2003a).

The age of the *jacutinga* mineralization is not well constrained. Lead isotopic data for palladian gold, quartz, specular hematite and martite (pseudomorphic hematite after magnetite) sampled at Cauê mine (Itabira district) were interpreted by Olivo et al. (1996) to define a Pb–Pb isochron corresponding to a late Transamazonian age of 1.83 ± 0.10 Ga. These lead data, however, show considerable excess scatter in the $^{207}Pb/^{204}Pb$ vs. $^{206}Pb/^{204}Pb$ diagram (MSWD = 7.55). Even more striking, the four samples with the most radiogenic Pb fall below the 1.83 Ga reference isochron (Olivo et al. 1996), which indicates that the Pb isotope systematics of these samples was disturbed during a younger event.

Crosscutting relationships also place uncertainties to the interpretation by Olivo et al. (1996). At Gongo Soco, *jacutinga* veins truncate mesoscopic folds with E–W-trending axes (Fig. 2a) and palladiferous gold itself cuts foliation-forming (S_2) platy hematite (Fig. 2b). These obliterated fabrics are ascribed to the Brasiliano orogeny (Chemale et al. 1994; Rosière et al. 2001). Similarly, jacutinga veins from Itabira crosscut the myonitic S_1-foliation (Fig. 2c) and palladiferous gold per se encloses and eventually transets platy hematite (Fig. 2d); i.e., specularite sensu Rosière and Rios (2004). According to these authors, specularite hematite crystals formed during the Brasiliano orogeny in domains of intense deformation with the development of a pervasive schitosity (S_1-foliation).

A Brasiliano age has been assumed for the palladian gold-bearing *jacutinga* veins (Guimarães 1970; H.F. Galbiatti unpublished Msc Thesis; Varajão et al. 2000). Some authors considered that the Brasiliano tectonic evolution had an important influence on the metallogenesis of the QF. This is illustrated by the development of foliated hematite fabrics in itabirite and associated high-grade hematite orebodies (Rosière et al. 2001). With regard to gold mineralization, late Brasiliano collapse tectonics produced extensional domains that coincide with auriferous quartz veins in the Ouro Preto area (Chauvet et al. 1994, 2001).

The Gongo Soco *jacutinga*-bearing itabirites are located in the north-western part of the Gandarela Syncline (Fig. 1), a major overturned structure (Moore 1969). The Cauê Formation at Gongo Soco is between 300 and 400 m thick. It strikes generally at 078–083°, and dips about 45°S. Both the enclosing itabirite and the high-grade soft hematite orebody have a prominent metamorphic foliation, defined by the planar orientation of hematite (platy hematite). Slightly discordant to the strike of the enclosing itabirite, the soft hematite deposit is spindle-shaped in plan, about 1,300 m long, up to 200 m wide, and trends at an azimuth of about 110°, plunging gently eastward. For a geological map, see Cabral et al. (2003b).

The world-class Itabira iron ore district is situated in the north-eastern extremity of the QF (Fig. 1), within a regional-scale syncline with subsidiary synclines (Chacrinha and Periquito; Dorr and Barbosa 1963). High-grade hematite ores and palladian gold-bearing, vein-style *jacutinga* mineralization at Itabira are hosted by itabirites of the Cauê Formation. In contrast to Gongo Soco, the Caraça Group is missing at Itabira (Chemale 1987) and the itabirite unit (Cauê Formation) directly rests tectonically on the greenstone rocks of the Archean Rio das Velhas Supergroup (Chemale et al. 1987; Olivo et al. 1995). There are three generations of structures at Itabira: (1) pervasive S_1 mylonitic foliation and E–W-trending stretching lineation, (2) S_2 axial planar foliation, mesoscopic folding with E–W-trending axis and strike-slip faulting, and (3) N–S-trending crenulation cleavage and reverse brittle faults (Chemale et al. 1987, 1994; Hasui et al. 1994; Olivo et al. 1995). Some authors consider these structures to be related to a W-verging thrusting event of Brasiliano age (Chemale et al. 1994; Rosière et al. 1997; Hackspacher et al. 2001). Oxygen isotope data indicate a temperature of 660°C for peak metamorphism at Itabira (Hoefs et al. 1982), whereas mineral assemblages suggest a lower metamorphic grade (Dorr and Barbosa 1963; Chemale et al. 1994; Pires 1995).

Quartz–hematite veins barren in palladian gold, but similar to *jacutinga*-style mineralization are known from the Córrego do Feijão and Fábrica iron ore deposits (Fig. 1). The Córrego do Feijão deposit is located in the western part of the NE–SW-trending, 100 km long Serra do Curral (serra = mountain chain). The rocks in the western Serra do Curral were metamorphosed under low-grade conditions, i.e. *grunerite* zone of Pires (1995),

with local superposition of thermal aureoles around granite-gneiss domes (Marshak et al. 1992). Córrego do Feijão is within the low-strain domain of the QF, which is characterized by discontinuous shear zones and thrust faults attributed to the Brasiliano orogeny, with relatively thick and diffuse zones of cohesive cataclasites (Rosière et al. 2001). The Fábrica iron ore mine (Fig. 1) is situated within the cummingtonite zone (Pires 1995). Fábrica is localized in a transition zone between the high- and low-strain domains. Although several Brasiliano thrusts occur in the Fábrica area, the platy hematite-defined schistosity (S_1) is weak or even absent due to the low internal strain undergone by the iron formation (itabirite) and high-grade iron ore orebodies under lower temperature conditions (Rosière et al. 2001).

Samples and analytical methods

Samples of quartz and specular hematite were selected from the Gongo Soco and Itabira *jacutinga*-style vein mineralization and from barren specular hematite-quartz veins exposed in the Córrego do Feijão and Fábrica iron ore deposits (Fig. 1). Aggregates of massive and irregular-shaped palladian gold (0.5–3.5 g) were recovered from a Knelson concentrator at the Gongo Soco iron ore plant.

Quartz-hosted fluid inclusions were measured by conventional microthermometry using a Linkam THMSG 600 heating and freezing stage with a TMS 93 temperature programmer. The stage was calibrated with synthetic inclusions supplied by Synflinc. Fluid inclusions hosted in chips of specular hematite (NB: no doubly polished wafers could be prepared from hematite samples) were studied using a U.S.G.S. heating-freezing system by Fluid Inc. with an Olympus BHSM-IR infrared microscope (Lüders 1996). The infrared image is transmitted to a monitor by an infrared camera. For freezing runs a Hitachi KP-161 CCD camera was used which allows observations in the near infrared spectral range to about 1200 nm. Since the IR transmittance of the studied hematite samples progressively decreases with increasing temperature for heating runs, the CCD camera was replaced by a high-resolution Hamamatsu C-2400 infrared TV camera with a tube that has a maximal detection capacity of about $\lambda \leq 2400$ nm (camera signal output current ≥1 nA for 500 μW). For calibration, synthetic standards and natural inclusions were used.

Gas-bearing inclusions in quartz from Itabira were analyzed with a Jobin-Yvon (formerly Dilor) Raman spectrometer. The exciting radiation used was from a 532 nm Nd/Yag laser.

Chemical analysis of fluid inclusions in quartz and hematite was carried out at the University of Leeds using the bulk crush-leach method as detailed in Banks et al. (2000). Quartz and hematite samples were crushed to between 1 and 2 mm grain size and the quartz samples boiled in aqua regia, followed by nitric acid. All samples were then boiled several times in 18.2 MΩ water and dried prior to analysis. Approximately 0.5 to 1 g of material was crushed, transferred to a suitable container and leached with 18.2 MΩ water for anion and Na, K and Li analysis or in acidified $LaCl_3$ solution, for analysis of other cations. Anions were determined by ion chromatography, Na, K and Li by flame emission spectroscopy, and other cations by inductively coupled plasma mass spectroscopy. Replicate analyses show the precision to be on average 5% RSD for the analysis of these samples.

For Pb isotope analysis (performed at GFZ, Potsdam), hematite samples were selected according to type of fluid inclusions. The samples were cleaned in 7 N HNO_3 and subboiling double-distilled H_2O (DDW), weighted and ground in an agate mortar (samples were covered with DDW). Powder and water were separated using a centrifuge and transferred into teflon beakers. They were dried before a mixed ^{205}Pb–^{235}U tracer was added. Samples were dissolved with 52% HF overnight at 160°C on a hot plate. Digested samples were dried and taken up in 6 N HCl. Pb and U were purified, passing the samples twice over 500 µl ion-exchange columns filled with AG1-8X, using the procedure described in Romer et al. (2005). Pb and U were loaded together with silica gel and H_3PO_4 on single Re-filaments. The isotopic composition of Pb was determined at 1,200–1,260°C using Faraday collectors in static multicollection on a Finnigan MAT 262 multi-collector mass-spectrometer. The isotopic composition of U was determined on the same instrument at 1280–1350°C using Faraday collectors in static multicollection.

Samples of palladian gold (analyzed at University Giessen) were precleaned using several alternating 6 N HCl and DDW washes over a period of 2 weeks. After final rinsing with acetone and drying, the samples were weighed into teflon screw-top beakers and dissolved in aqua regia on a hot plate. The solutions were split into two aliquots for separate determination of Pb isotope ratios and Pb concentrations by isotopic dilution using a ^{206}Pb tracer. Lead was separated using EICHROM Sr resin on 250 µl teflon columns. After washing with 3 N HNO_3 and DDW, Pb was eluted with 6 N HCl. The Pb eluate was further processed through a 250 µl column containing EICHROM Pre Filter Resin. The entire procedure was repeated using 50 µl columns to purify Pb. For mass spectrometry, Pb was loaded onto single Re filaments using silica gel–H_3PO_4 bedding. All isotopic ratios were determined on a six-collector Finnigan MAT 261 solid-source mass-spectrometer running in static multicollection.

Results and interpretation

Fluid inclusion petrography

Quartz

Quartz samples from Gongo Soco contain numerous trails and clusters of aqueous fluid inclusions of highly

variable shape and size. Due to the high number of inclusions in the studied samples, a clear classification, i.e., primary vs. secondary origin of the inclusions, is often impossible. The majority of quartz-hosted fluid inclusions have irregular shape and are between 20 and 60 μm large. Rounded inclusions are less abundant and smaller (15–30 μm). Fluid inclusion data were obtained from some isolated inclusions that appear to be primary in origin according to the criteria of Roedder (1984). Monophase aqueous inclusions are always arranged along healed cracks and, therefore, can be classified as secondary inclusions.

Two compositional types of fluid inclusions were observed in quartz samples from the Itabira district. These are (type 1) aqueous carbonic inclusions or multiphase aqueous (± carbonic) inclusions with at least

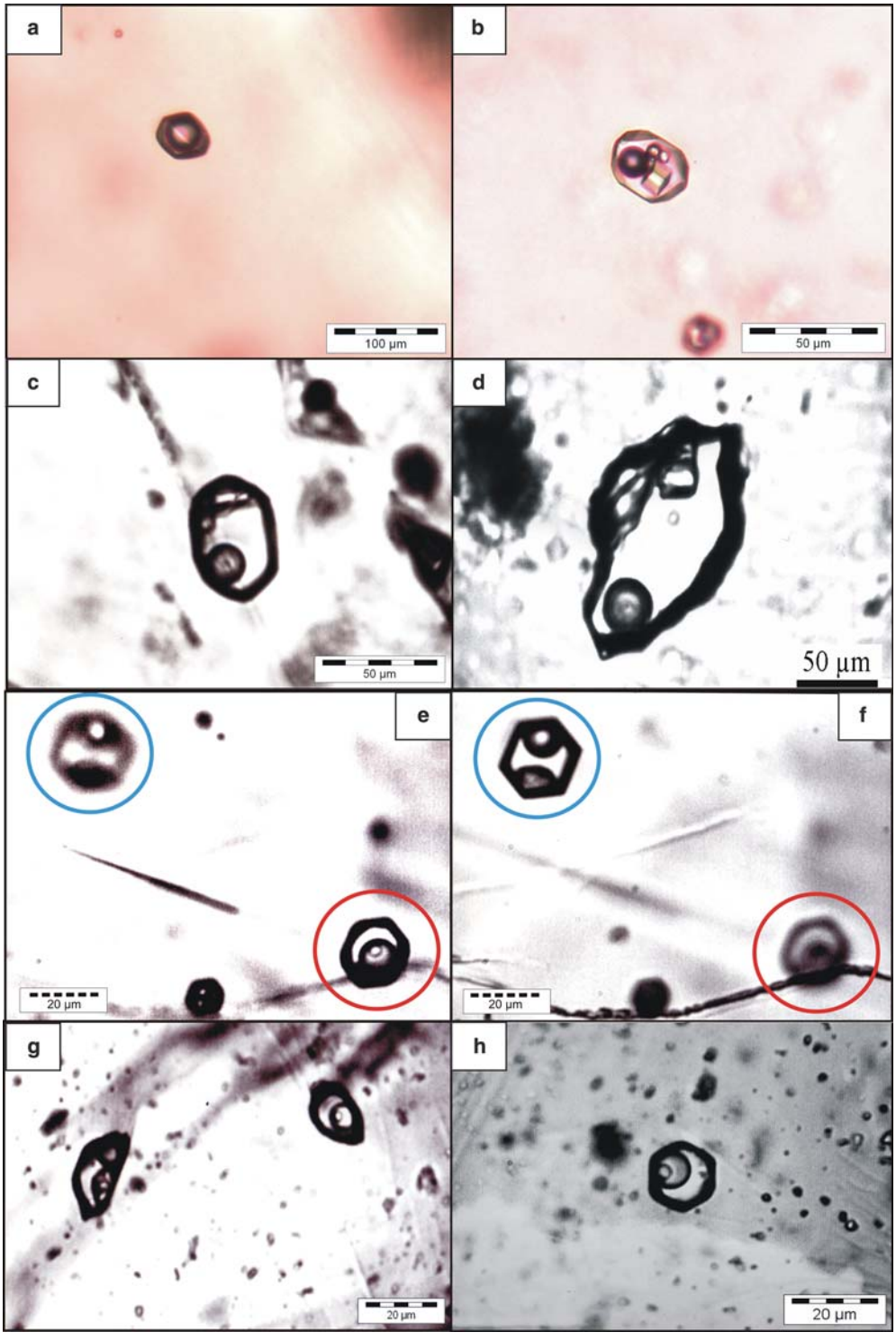

Fig. 3 Photomicrographs of fluid inclusions trapped in quartz and specular hematite samples. **a** Vapor-rich (CO_2 + N_2) inclusion from a cluster of primary (?) inclusions in quartz, Itabira. **b** Multiphase aqueous (±carbonic) inclusion with a cubic halite (?) daughter crystal and two additional solids (sulfates) in quartz from the same cluster as (**a**), Itabira. **c**–**h**. Transmitted IR light microphotographs of fluid inclusions in specular hematite. **c** Aqueous fluid inclusion with solids of unknown composition in specular hematite from a barren vein in the low-strain domain of the QF, Fábrica. **d** Aqueous fluid inclusion with a solid of unknown composition in specular hematite from a *jacutinga*-style vein, Gongo Soco. e, f) Negative crystal-shaped aqueous fluid inclusion with a solid (*blue circle* in e and **f** and aqueous-carbonic inclusion (*red circle* in **e** and **f** in a specular hematite grain, Itabira. **g** Aqueous fluid inclusion with solids and aqueous-carbonic inclusion in specular hematite, Itabira. **h** Aqueous-carbonic inclusion with a small solid from a cluster of multiphase aqueous and aqueous-carbonic inclusions

one solid phase (Fig. 3a, b) and (type 2) two-phase aqueous or monophase aqueous inclusions. Type 2 inclusions are always arranged along trails crosscutting quartz, probably due to healing of secondary cracks. These secondary inclusions rarely contain a solid phase. Type 2 inclusions are very abundant in the studied samples, whereas type 1 inclusions only occur in isolated clusters and, therefore, are interpreted to be primary or pseudosecondary (cf. Roedder 1984). Some planes contain dark gas-rich or multiphase inclusions showing negative crystal shape. At room temperature, type 1 inclusions consist of two (liquid $H_2O + CO_2$ supercritical fluid) or three (liquid H_2O + liquid CO_2 + CO_2-rich vapour) phases (Fig. 3a, b). The carbonic phase occupies 15–60 vol.% of the inclusions. Type 1 inclusions may contain up to three solid phases (Fig. 3b). These solid phases, however, are differently composed. Some type 1 inclusions contain salt crystals, i.e. cubic halite crystals and most probably sylvite that show no Raman signal. Other type 1 inclusions host solid crystals with a strong Raman peak at 1084.4 cm^{-1}, characteristic of calcite (e.g., Burke 1994). Raman vibration lines at 622.4, 627.5, 1005.4, 1013.9 and 1,104.9 cm^{-1} indicate that rare solid phases hosted in aqueous type 2 inclusions most probably are sulfates (gypsum and anhydrite?).

Hematite

With the exception of martite samples from hematite veins in the NW part of the Itabira district, samples of specular hematite display an excellent transparency for near infrared radiation, similar to hematite from the Kalahari manganese field, South Africa (Lüders et al. 1999). Hematite from barren veins of the Fábrica and Córrego do Feijão iron ore mines contain only one compositional type of fluid inclusions. These are aqueous inclusions with a vapor bubble and, at least one solid phase in more than 90% of all observed inclusions (Fig. 3c). Hematite-hosted fluid inclusions from the *jacutinga*-style mineralization of Gongo Soco are similar to those of barren veins and show irregular or rounded-elongated shape. They occur either as isolated inclusions or in clusters and appear to be of primary origin (Roedder 1984). The smallest inclusions are about 20 μm; but especially in samples from Gongo Soco exceptionally large inclusions exceeding 100 μm are abundant (Fig. 3d). Conspicuously, no trails of secondary fluid inclusions were observed in any of the studied samples. Fluid inclusions hosted in hematite from barren veins of Fábrica and Córrego do Feijão mostly occur in clusters. Since no crystal plains or growth zones could be observed in the specular hematite chips, a classification in primary vs. secondary origin is not straightforward.

Hematite samples from *jacutinga*-style mineralization at Itabira contain two compositional types of fluid inclusions, (1) aqueous carbonic inclusions (Fig. 3e, g, h), and (2) multiphase aqueous inclusions with at least one solid phase (Fig. 3f, g). Both types of inclusions occur together in isolated clusters or as isolated fluid inclusion pairs within individual samples (Fig. 3e–g). They show either irregular or hexagonal negative crystal shape, or rounded shapes within these individual clusters (Fig. 3e–h). The size of the aqueous carbonic inclusions (5–40 μm) is always smaller than those of associated multiphase aqueous inclusions (10–60 μm). Only in rare cases (in clusters with high abundance of both types of inclusions) it was observed that aqueous-carbonic inclusions may also contain a small solid phase (Fig. 3h). The liquid/vapour ratios are ~9 in multiphase aqueous fluid inclusions, whereas the volume fraction of the carbonic phase in aqueous carbonic inclusions is highly variable (~0.4–0.9).

Applying the definition of Goldstein and Reynolds (1984), aqueous carbonic and multiphase aqueous inclusions form fluid inclusion assemblages within individual clusters. Optically, it is not possible to decide whether this feature resulted from an immiscibility process in a single (supercritical?) fluid or from unmixing of two compositionally different fluids. It seems, however, very likely that both types of inclusions were trapped contemporaneously.

Fluid inclusion microthermometry

Quartz

Isolated two-phase fluid inclusions in quartz from Au–Pd–Pt-bearing quartz–hematite veins from Gongo Soco show ice melting temperatures in the range between −12.4 and −8.7°C (Table 1). This corresponds to a salinity of 12.5–16.3 wt.% NaCl equivalent. The homogenization temperatures fall into the temperature range between 74.3 and 130.6°C (Table 1). The homogenization and ice melting temperatures of secondary aqueous type 2 inclusions in quartz samples from the Itabira district are similar to the data obtained from fluid inclusions in quartz from Gongo Soco (Table 1). In contrast, aqueous carbonic (type 1) inclusions show lower ice melting temperatures than secondary aqueous type 2 inclusions. Most of the carbonic inclusions decrepitate prior to total homogenization. The homogenization temperatures obtained are considerably higher than those of the fluid inclusions in quartz from Gongo Soco and cover the temperature range between 230 and 360°C (Table 1). Laser Raman analyses prove the presence of CO_2 and N_2 in the gas phase of type 1 inclusions. The CO_2 and N_2 content varies between 88.1–95.2 mol% and 4.8–11.9 mol%, respectively. Other gases were not detected by Raman spectroscopy.

Hematite

Aqueous two-phase fluid inclusions and multiphase aqueous inclusions with solid phases in specular hematite from *jacutinga* veins of the Gongo Soco mine as well as from barren veins from Fábrica and Córrego do

Table 1 Summary of microthermometric data of fluid inclusions in quartz and specular hematite from quartz–hematite veins

Location	Material	FI type	Te (n)	Tm ice (n)	Tm hydrate (n)	Th (n)	Tm CO_2 (n)	Tm clath. (n)	Th CO_2 (n)
Gongo Soco	Quartz	2-phase	−38.1 to −32.2 (5)	−12.4 to −8.7 (15)	NM	74.3 to 130.6 (15)	NM	NM	NM
Gongo Soco	Hematite	Multiphase	−30 to −28 (12)	−8 to − 6.2 (31)	NM	148.1 to 167.4 (15)	NM	NM	NM
Fábrica	Hematite	Multiphase	−28 (2)	−9.8 to −7.5 (6)	NM	217.9 to 228.9 (6)	NM	NM	NM
Córrego d. F.	Hematite	Multiphase	−29 to −27.5 (3)	−7.3 to −4.5 (16)	NM	189.3 to 203.8 (16)	NM	NM	NM
Itabira	Quartz	2-phase	−38 to −35.2 (32)	−15.3 to −11.8 (35)	NM	128.7 to 154.8 (35)	NM	NM	NM
Itabira	Quartz	Aq.-carb.	−42.1 to −35 (20)	−24.5 to −22.5 (23)	−10.6 to −7.3 (7)	230.1 to 359.8 (10)	−61.5 to −57.4 (23)	4.5 to 8.3 (12)	18.1 to 21.6 (23)
Itabira	Hematite	Multiphase	−38.2 to −33.5 (6)	−27 to −14.3 (30)	−11.3 to −10 (4)	275 to 362.3 (30)	NM	3.9 (1)	NM
Itabira	Hematite	Carbonic	−35 to −34 (2)	−15.6 to −10.7 (24)	NM	335.6 to 468.7 (24)	−62.9 to −56.7 (24)	11.6 to 15.9 (4)	14.2 to 27.8 (24)

NM not measured

Feijão show narrow ranges of salinity and homogenization temperature (Fig. 4 and Table 1). In some cases first melting was observed around −30°C for fluid inclusions hosted in samples from Gongo Soco and −27°C in samples from Córrego do Feijão. The highest salinities (11.1–13.7 wt.% NaCl equivalent derived from final ice melting temperatures) and homogenization temperatures (218–229°C) of these deposits were measured in fluid inclusions hosted in barren hematite from the Fábrica mine (Table 1).

Fluid inclusions hosted in specular hematite from the Itabira area are more complex. The ice melting temperatures of multiphase aqueous inclusions cover a wide range between −26.1 and −10.7°C (Table 1). In

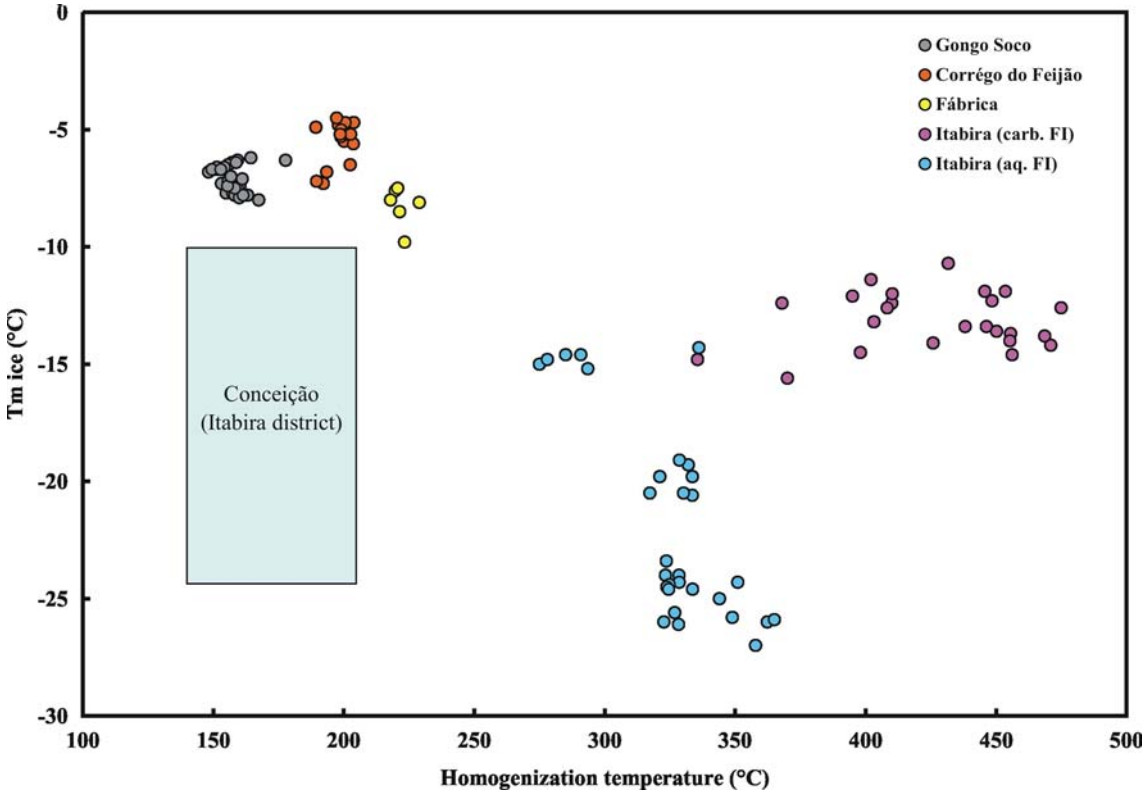

Fig. 4 Th vs Tm_{ice} diagram of fluid inclusions in specular hematite from auriferous (*jacutinga*) and barren veins in the QF. The blue box comprises the range of Th vs. Tm_{ice}values measured in specular hematite from the Conceição deposit (Rosière and Rios 2004) in the high-strain domain

some instances, sluggish melting of a second phase (most probably hydrohalite) at temperatures between −11.5 and −9.5°C was observed as well. First melting was observed around −35°C in some inclusions (Table 1). Melting of clathrate (between +3 and +8°C) in multiphase aqueous inclusions was only observed in two inclusions hosted in a cluster where associated aqueous-carbonic inclusions were abundant. Homogenization temperatures of multiphase aqueous inclusions are mostly between 317 and 365°C (Fig. 1). Only one sample from the Cauê mine (Fig. 1) hosts multiphase aqueous fluid inclusions showing higher ice melting temperatures between −15.2 and −14.6°C (no hydrohalite melting was observed in these inclusions) and lower homogenization temperatures between 275 and 293.5°C (Fig. 4).

In contrast, aqueous carbonic inclusions have higher ice melting temperatures and considerably higher total homogenization temperatures compared to multiphase aqueous inclusions (Fig. 4; Table 1). It is noteworthy that very gas-rich inclusions are too dark to observe any phase transitions therein. Microthermometric data could only be obtained from aqueous carbonic inclusions with volume fractions of <0.7 carbonic phase.

The ice melting temperatures fall into the temperature range between −14.6 and −10.7°C (Table 1). Melting of hydrohalite was not observed. However, melting of clathrate was observed in a few inclusions in the temperature range between +12.4 and +16.3°C. The melting temperatures of CO_2 range between −56.6 and −62°C, but mostly around −58°C. Most of the measured Tm CO_2 ice values are lower than the triple point of pure CO_2. Therefore, small concentrations of additional volatile species, probably N_2 (as indicated by Raman analyses of gas-rich inclusions in associated quartz) may be present in the gas phase. Homogenization temperatures of the CO_2 phase into the liquid lie between +14.2 and +27.8°C (mean +20.2°C; $n=24$).

Melting of the solid phase(s) was never observed in any multiphase aqueous inclusions, even upon heating the samples to temperatures as high as 600°C. However, it is remarkable that none of the inclusions (even carbonic inclusions) decrepitated upon heating to such high temperature.

Rosière and Rios (2004) studied specular hematite-hosted fluid inclusions from high-grade hematite ore of the Conceição deposit in the western part of the Itabira district (Fig. 1). In contrast to the results of this study, they observed only aqueous and multiphase fluid inclusions in hematite, whereas the occurrence of aqueous carbonic inclusions was restricted to late vein quartz of uncertain age. Multiphase aqueous fluid inclusions from the Conceição deposit showed ice-melting temperatures in approximately the same temperature range as multiphase inclusions from other veins in the Itabira district, but the homogenization temperatures were considerably lower (Fig. 4).

Crush-leach analysis

The results of the crush-leach analyses on samples of quartz and hematite are presented in Table 2. The data show that Cl and SO_4 are the major anions in quartz- and hematite-hosted fluid inclusions. Fluoride was not detected. The fluids are dominated by Na and have significant but variable amounts of K and Ca, and lesser amounts of Mg and Li (Table 2).

Table 2 Crush-leach analyses of fluid inclsuions hosted in quartz and specular hematite from occurrences in the QF. Anion and cation data reported in ppb (as analyzed)

Sample no.	Locality	Material	Na	K	Li	Cl	Br	SO_4	Ca	Mg	Sr	Fe
PQ-535	Gongo Soco	Quartz	2915	779	20.5	4,721	50.6	1,091	331	95	5.7	92
PQ-835	Gongo Soco	Quartz	3509	905	9.1	4,626	30.1	1,003	286	79	6.5	170
PS-44	Gongo Soco	Quartz	704	201	2	1,230	15.1	1,427	NA	NA	NA	NA
PS-17 Qz	Gongo Soco	Quartz	1188	334	8	1,749	9	405	NA	NA	NA	NA
PQ-892 Qz	Gongo Soco	Quartz	1386	461	10	2,246	8.6	1,330	NA	NA	NA	NA
PQ-883 Qz	Gongo Soco	Quartz	902	519	2.4	1,441	6.2	332	NA	NA	NA	NA
PQ-535 Qz	Gongo Soco	Quartz	440	205	2.1	671	5.6	184	NA	NA	NA	NA
Y-66	Itabira	Quartz	1,210	363	1	2,078	15.9	356	NA	NA	NA	NA
Y-67	Itabira	Quartz	220	89	1.1	364	1	546	NA	NA	NA	NA
865	Cauê/Itabira	Quartz	341	102	0.2	638	1.9	609	NA	NA	NA	NA
NW	Itabira	Quartz	231	278	0.8	421	1.2	110	NA	NA	NA	NA
Lico-875-3 Qz	Itabira	Quartz	319	300	1.5	640	5	126	NA	NA	NA	NA
Y-725-Qz	Itabira	Quartz	125	187	0.8	222	2.2	80	NA	NA	NA	NA
740/3 Qz	Itabira	Quartz	275	188	1.2	469	4.6	51	NA	NA	NA	NA
FA-08	Fábrica	Hematite	506	157	1.9	866	6.7	576	94	11	7	NA
CF-1130	Córrego do Feijão	Hematite	6,897	1,538	48	11,972	129	3,206	1,121	108	17	NA
865	Itabira	Hematite	4,818	945	10.2	7,216	77.1	1,924	471	54	25	NA
Y-66	Itabira	Hematite	1,540	396	23	3,165	45.7	1,128	289	26	15	NA
Y-67	Itabira	Hematite	814	360	5	1,279	8.1	1,845	365	46	8	NA
LICO	Itabira	Hematite	484	806	2.5	680	1.3	1,108	265	26	6	NA
NW	Itabira	Hematite	583	785	6.6	989	6.3	831	125	15	7	NA
740/3 Hem	Itabira	Hematite	847	271	11	1,493	7.4	349	NA	NA	NA	NA

NA not analyzed

In the absence of evaporitic minerals, Cl and Br behave conservatively during fluid flow and are not significantly involved in fluid–rock interactions. Therefore, Cl/Br ratios of fluid inclusions can provide information on the origin of salinity in brines (Banks et al. 1991; Böhlke and Irwin 1992). There is a large variation in the Cl/Br and Na/Br ratios of the fluid inclusions even in paired samples of quartz and hematite (Fig. 5). This could be attributed to the high abundance of secondary inclusions with different fluid compositions in quartz or to the fact that quartz and hematite precipitated from fluids of different composition. The Cl/Br and Na/Br ratios of most of the fluids are lower than those of seawater, normally taken as an indication of halite saturation during seawater evaporation (Fig. 5). The analyzed fluids, however, do not plot on the seawater evaporation line. Normally, fluids that do not lie on the seawater evaporation line are the result of water–rock interaction (WRI), when Na in the fluid is exchanged for another cation, and they plot to the left of the line. Here, the fluids plot to the right along a 1:1 line in Fig. 5 that would have halite as one end-member (Cl/Br halite of about 20,000). The low Cl/Br and Na/Br ratios are indicative of halite dissolution and reprecipitation by a halite-saturated fluid. During dissolution and reprecipitation, Br is excluded from halite and enriched in the fluid, just as during halite precipitation from seawater. The salinity of the fluid inclusions, however, is below halite saturation and indicates dilution after they have gained Br by interaction with halite. Leaching of organic-rich sediments to increase the Br and lower the Cl/Br and Na/Br ratios in the fluids seems to be an unlikely option because the fluids would then not lie beneath the seawater evaporation line. Three samples from the Itabira district exhibit Cl/Br ratios higher than seawater, which is probably due to dissolution of evaporite layers that are locally present within the itabirite unit.

The Na/K ratios of the analyzed fluids fall into a narrow range between 1 and 8.5 (mean 4.5 ± 2.2, Fig. 6). The Na/K ratios in brines are likely to be controlled by equilibrium reactions with alkali feldspars and muscovite. The range of temperatures of the parental ore-forming fluid as indicated by the Na/K and Na/Li ratios is approximately 340 ± 40°C (Verma and Santoyo 1997). Despite this apparently large range in elemental ratios, they probably reflect conditions close to equilibrium. Therefore, the elevated K and Li concentrations in the fluids (Table 2) are likely to derive from water/rock interaction between the ore-forming fluids and granites and/or gneiss in the crystalline basement. Significant amounts of SO_4 are unusual for crustal fluids, but are typical of fluids that dissolved gypsum (from evaporites) or near-surface fluids that received sulfate from bio-oxidation of pyrite. Due to the high homogenization temperatures of the fluid inclusions, the latter source is very unlikely. Fluids with high contents of K and SO_4 may also be produced from H_2S acid or sulfide-bearing fluids (similar to those present in modern acid geothermal systems) that have altered feldspars and were oxidized close to the surface. The variable Na/Br and Cl/Br ratios of the fluid inclusions in quartz and hematite (Fig. 5) could be indicative of immiscibility of a supercritical fluid. The highest Cl/Br ratios were detected in samples from the high-grade metamorphic terrain where

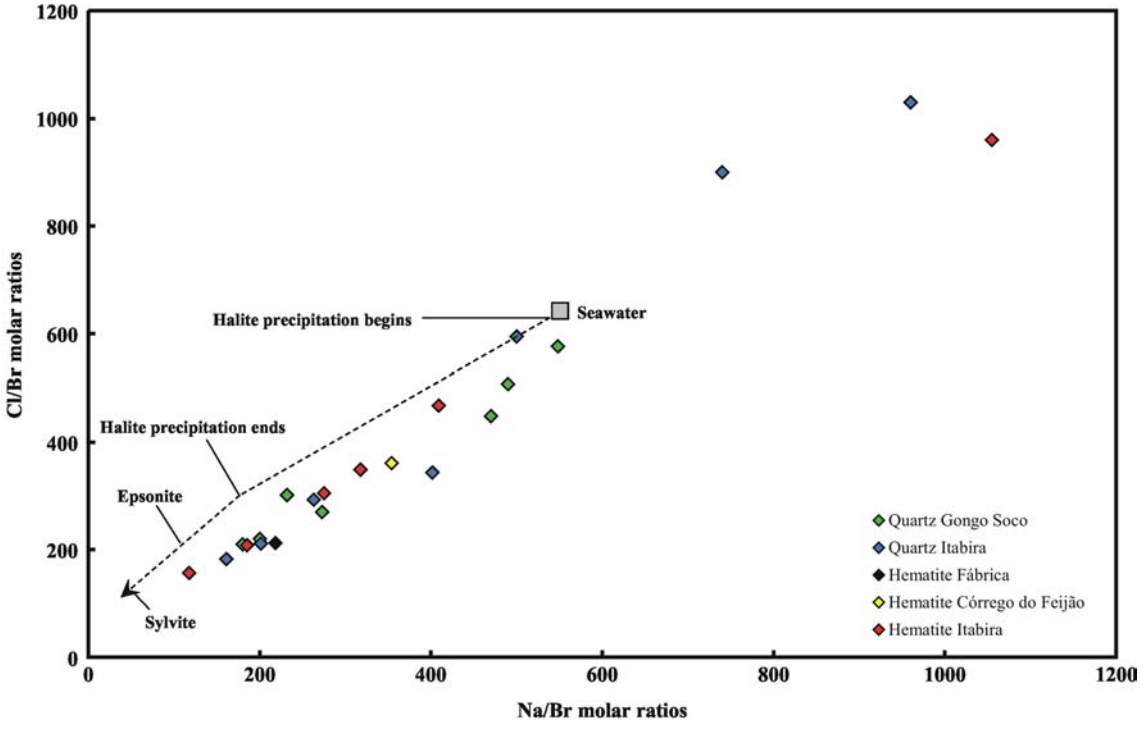

Fig. 5 Na/Br vs Cl/Br diagram. Reference line for Na:Cl = 1:1 (for details see text)

aqueous fluid inclusions occur in the same clusters along with carbonic inclusions. Immiscibility of a supercritical fluid, therefore, cannot be excluded to explain the varying Cl/Br ratios.

U–Pb systematics of hematite, hematite-hosted fluid inclusions and palladian gold

The initial Pb isotopic composition of a primary fluid inclusion and its host mineral is identical. If inclusion and host mineral remained closed systems and had different Pb/U ratios, they may be used to construct two-point isochrons. Following this approach, we separated hematite with different types of fluid inclusions. The fluid inclusions were released and separated from the hematite powder. Thus, we obtained a sample pair for each hematite fraction consisting of an inclusion-free hematite residual and a corresponding fluid inclusion leachate.

The use of U–Pb systematics of fluid inclusions and their hematite host for dating is based on the different behavior of U and Pb in fluids and their contrasting potential to enter the crystal lattice of hematite. Fluids can carry significant amounts of Pb and, depending on their oxidation state, also important amounts of U. Therefore, fluid inclusions may have $^{238}U/^{204}Pb$ values that range from very small values to large values. In contrast, the crystal lattice of hematite cannot easily accommodate Pb, which has a too large ionic radius. U^{6+}, however, is readily accommodated in the crystal structure of hematite as U^{6+} has the same ionic radius as Fe^{3+} (Shannon 1976). Thus, hematite is expected to have $^{238}U/^{204}Pb$ values that generally are higher than those of the fluid inclusions. These expectations were fulfilled by the hematite samples from *jacutinga*-style mineralization of Itabita and Gongo Soco. Depending on sample and type of fluid inclusion, the fluid inclusions usually contain between 0.8 and 5.3% of the total Pb and 0.5 and 11% of the total U contained in the sample (Table 3). Typically, the portion of Pb is higher than the portion of U, which suggests that U in most samples fractionated more readily into the hematite crystal than Pb did. Less than 1% of the total volume of the crystal is made up by fluid inclusions, which have a much lower density than the host. Thus, although the Pb and U contributions from the fluid inclusions are small, the absolute concentrations of Pb and U in the fluid inclusions are higher than in the host hematite.

Hematite

The Pb isotope data of the hematite samples scatter widely in the $^{206}Pb/^{204}Pb$ vs. $^{207}Pb/^{204}Pb$, $^{206}Pb/^{204}Pb$ vs.

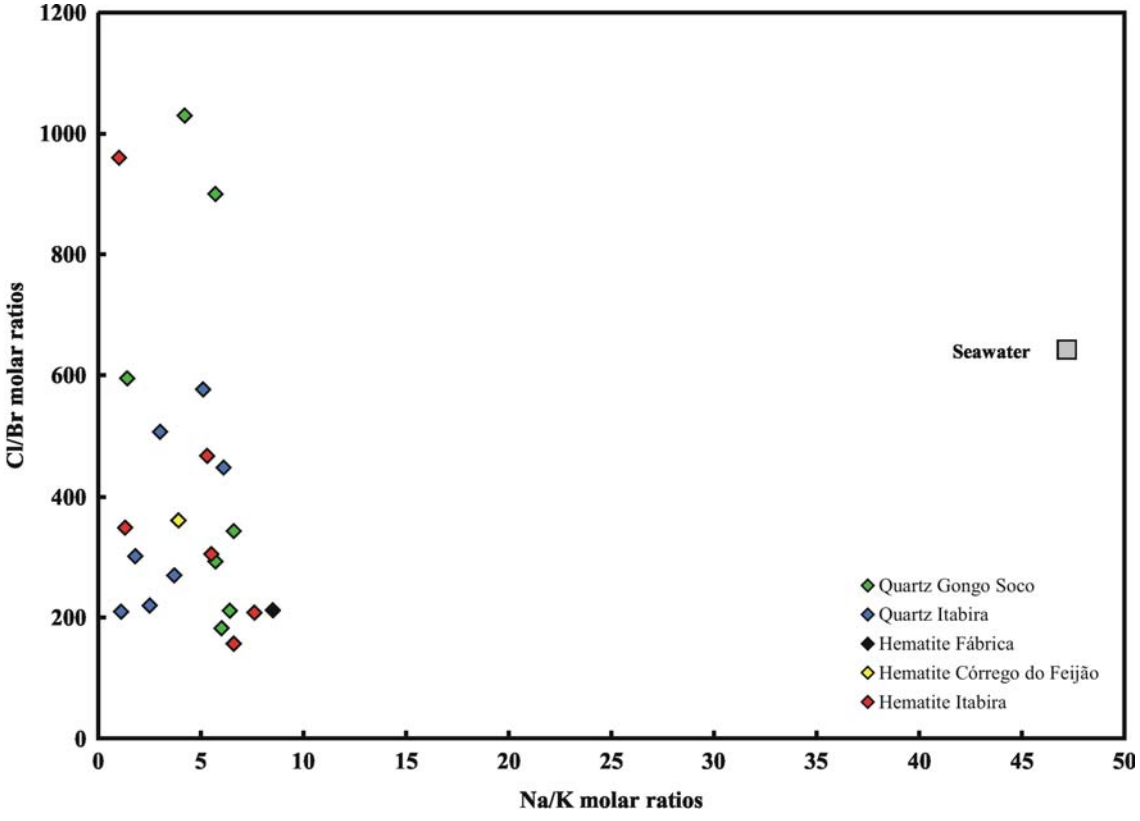

Fig. 6 Na/K vs. Cl/Br diagram. The narrow range of the Na/K ratios (mean 4.5 ± 2.2) but variable Cl/Br ratios can be due to fluid immiscibility (see text)

$^{208}Pb/^{204}Pb$ and $^{206}Pb/^{204}Pb$ vs. $^{238}U/^{204}Pb$ diagrams (Fig. 7a-c). The data do not define isochrons. Although the scatter among samples from individual deposits is smaller than for the entire data set, there is significant excess scatter, which may originate from (1) initial isotopic heterogeneity within single deposits and contrasting Pb composition in different deposits, (2) addition of isotopically distinct Pb at some time after formation of the deposits, and (3) fractionation between U and Pb (modification of the $^{238}U/^{204}Pb$ ratio) during a later event. Furthermore, there may have been some redistribution of radiogenic Pb by α-recoil, i.e. by implantation of daughter isotopes from the fluid inclusions into the hematite structure or expulsion from the hematite into the fluid inclusions (Romer 2003; Romer and Rocholl 2004). These circumstances make the derivation of a precise age impossible. Nonetheless, the Pb isotope systematics of the fluid-free hematite samples impose several constraints on the evolution of the hematite veins.

1. The data fall in a triangular area in the $^{206}Pb/^{204}Pb$ vs. $^{207}Pb/^{204}Pb$ diagram (shaded area, Fig. 7a), which may reflect a heterogeneous source or a poly-stage evolution of the hematite veins. Samples defining the flattest and steepest slope in the $^{206}Pb/^{204}Pb$ vs. $^{207}Pb/^{204}Pb$ diagram yield a maximum and a minimum age, respectively, for different aspects of the evolution of the deposits. The flattest $^{207}Pb/^{206}Pb$ trend with a slope of 0.067 corresponds to an

Table 3 Pb isotope data of hematite and its fluid inclusions, Quadrilátero Ferrífero, Brazil

Sample[a]	Pb[b] (ppm)	Pb[c] (ng)	U[c] (ng)	$^{206}Pb^{d}$ ^{204}Pb	$^{207}Pb^{d}$ ^{204}Pb	$^{208}Pb^{d}$ ^{204}Pb	$^{238}U^{d}$ ^{204}Pb	f_U^e	f_{Pb}^e
Gongo Soco (aqu.)									
1-R	1.92	190	65.4	25.130	16.561	36.169	23.5		
1-L		156	8.16	21.746	16.408	36.278	3.40	0.008	0.451
Gongo Soco (078 PQ 892)									
2-R	0.948	106	50.8	25.872	16.592	36.370	37.6		
2-L		2.2	0.49	21.060	16.026	37.035	14.5	0.013	0.023
3-R	0.463	46	65.7	34.873	16.966	36.464	109		
3-L		0.4	0.45	26.597	16.325	37.036	88.6	0.026	0.048
4-R	1.21	119	41.3	24.255	16.546	36.060	23.3		
4-L		3.3	1.06	23.620	16.614	36.368	21.1	0.014	0.027
Córrego do Feijão									
5-R	1.73	542	86.8	43.810	17.672	37.950	81.7		
5-L		5.1	5.60	41.881	17.600	37.983	84.5	0.061	0.058
6-R	2.68	236	353	41.040	17.468	37.949	54.8		
6-L		3.2	2.77	35.909	17.274	37.927	43.1	0.008	0.009
7-R	1.90	236	229	41.861	17.443	37.934	82.5		
7-L		3.24	2.39	30.695	16.789	37.801	54.8	0.010	0.014
Fábrica									
8-R	1.81	317	32.0	20.154	15.990	37.004	6.47		
8-L		6.4	2.49	20.028	15.960	36.996	24.7	0.072	0.020
9-R	2.05	97.6	31.0	19.934	15.932	37.109	5.49		
9-L		2.4	1.20	19.730	15.898	37.260	17.2	0.037	0.012
10-R	1.64	92.1	11.3	19.887	15.896	37.057	7.39		
10-L		5.6	0.46	19.994	15.951	37.045	12.1	0.039	0.024
Itabiria (carb.)									
11-R	0.118	11.2	22.7	32.470	16.936	38.915	157		
11-L		11.7	2.82	22.167	16.206	36.984	15.8	0.110	0.512
12-R	0.136	14.6	33.1	36.375	17.049	36.828	179		
12-L		0.35	0.43	25.778	16.206	37.026	84.6	0.007	0.008
Itabiria (aqu.)									
13-R	0.190	27.3	59.7	35.696	17.068	36.816	171		
13-L		0.3	0.29	24.682	16.154	36.876	62.9	0.008	0.020
14-R	0.135	18.3	11.9	34.359	16.908	36.807	135		
14-L		0.9	0.332	23.483	16.330	36.877	23.6	0.025	0.027
15-R	0.192	11.1	20.5	33.091	16.886	36.776	139.4		
15-L		0.31	0.30	26.285	16.735	37.578	68.0	0.005	0.011

[a]Samples were selected to include only a single type of fluid inclusion
[b]Concentration data are calculated for the total sample (hematite + inclusions). In most cases, Pb is dominantly hosted in the hematite and, thus, the error originating from unaccounted Pb in the fluid inclusions is minor. Concentrations were determined by isotope dilution
[c]Total amount of Pb and U present in hematite and fluid inclusion, respectively. For comparison, the Pb blank is typically better than 15 pg Pb
[d]Isotope ratios were corrected for 15 pg Pb blank, tracer Pb, 1 pb U blank, and 0.1 %/A.M.U. mass discrimination
[e]Fraction of U and Pb originating from the fluid inclusions. $f_U = U_{fluid}/(U_{fluid} + U_{hematite})$; $f_{Pb} = Pb_{fluid}/(Pb_{fluid} + Pb_{hematite})$

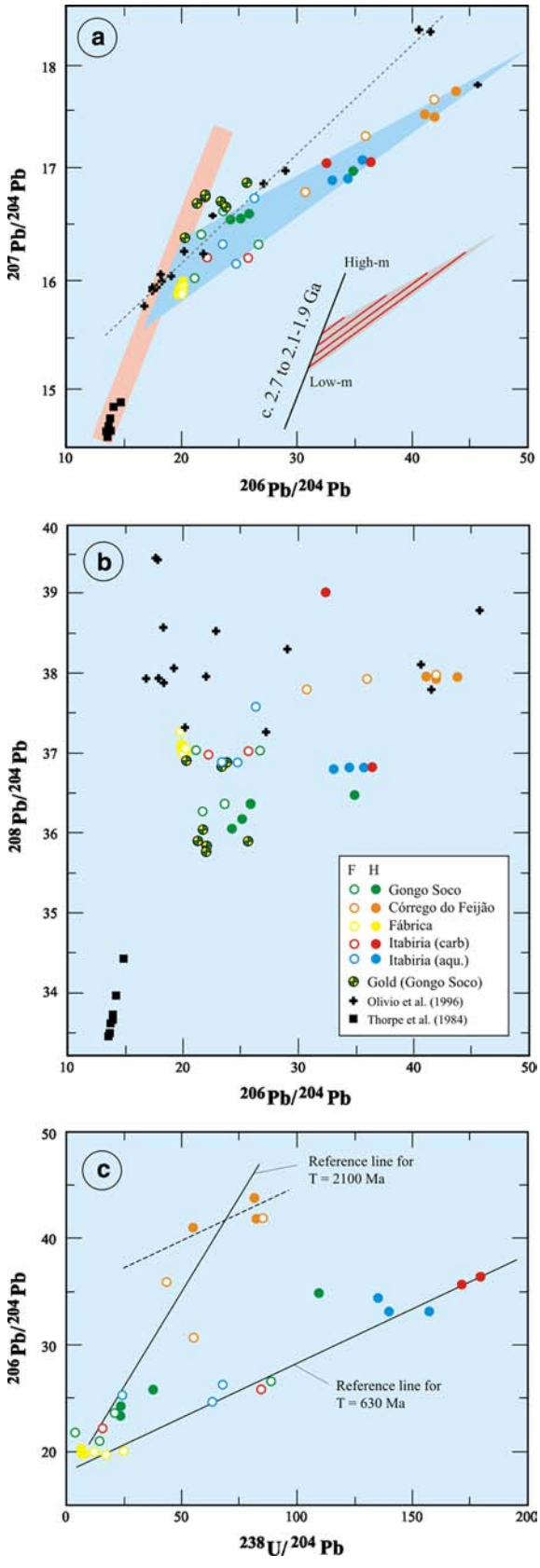

Fig. 7 Pb–Pb and U–Pb isotope systematics of hematite, gold and whole-rock samples. For each hematite sample, the fluid inclusion (Fl, *open symbols*) and the host hematite (Hm, *solid symbol*) were analyzed separately. Literature data include mineral analyses from wall rock and hematite analyses from the Cauê mine (Olivo et al. 1996) and from galena of Archean gold deposits in the Rio das Velhas Supergroup (Thorpe et al. 1984). Lead array through the Archean gold deposits corresponds to lead evolution from the deposition of the Archean supracrustal rocks to the Transamazonian orogeny. The dashed reference line denotes the 1.83 Ga age preferred by Olivo et al. (1996) for the Cauê mine. Note that this data set includes another three samples that have $^{206}Pb/^{204}Pb > 50$ and that fall below the reference line. The blue area includes all Pb isotope data from vein hematite. Note that Pb from gold samples has the lowest $^{208}Pb/^{204}Pb$ values and the host-rock samples the highest ones. Analytical uncertainties are smaller than symbol size, except for a few fluid inclusion samples with particular low total Pb contents

apparent $^{207}Pb/^{206}Pb$ age of ca. 800 Ma, which corresponds to a maximum age for the younger event. The steepest $^{207}Pb/^{206}Pb$ trend corresponds to an apparent age of ca. 2.0 Ga. Since the sampled *jacutinga*-style veins are hosted by the Paleoproterozoic itabirite (Cauê Formation) variations along the 2.7–1.9 Ga trend possibly reflects derivation of Pb from an isotopically heterogeneous source during the Paleoproterozoic formation of the iatbirite unit. Thus, the $^{206}Pb/^{204}Pb$ vs $^{207}Pb/^{204}Pb$ systematics may reflect either (1) Paleoproterozoic formation of the hematite veins and a Paleozoic reworking or (2) Paleozoic formation of the hematite veins with Pb derived from Paleoproterozoic source rocks.

2. In the $^{206}Pb/^{204}Pb$ vs. $^{238}U/^{204}Pb$ isochron diagram (Fig. 7c), all data from the *jacutinga*-style veins scatter about a linear trend, the slope of which corresponds to an age of ca. 630 Ma. This age has no strict geochronological meaning as the requirements for an isochron (common initial, single stage evolution) are not met. The samples from the barren Corrégo do Feijão veins fall above this Paleozoic reference line, which either implies that these samples had a more radiogenic initial Pb isotopic composition (this possibility is indicated by the 630 Ma reference line, Fig. 7c) or that they had a similar initial Pb isotopic composition as the other deposits, but record an older age (this possibility is indicated by the dashed reference line, Fig. 7c). Thus, the Pb isotopic constraints on the age of these barren hematite veins are ambiguous.The samples from the barren Fábrica veins are unradiogenic (Fig. 7c) and do not provide any age constraints.
3. Hematite from each deposit shows a relatively narrow internal range in $^{208}Pb/^{204}Pb$, whereas there are distinct differences between deposits (Fig. 7b). As there was little or no in-situ ^{208}Pb growth in hematite, i.e., $^{232}Th/^{204}Pb$ ratios were low, the internal correspondence of $^{208}Pb/^{204}Pb$ ratios within deposits suggests that Pb in each deposit was derived from individual sources.
4. The initial Pb isotopic composition of all deposits seems to have been relatively radiogenic ($^{206}Pb/^{204}Pb$ *approx* 18–19.5) with high $^{207}Pb/^{204}Pb$ values, which

implies that the initial Pb of the hematite deposits was dominantly derived from an old crust.

Fluid inclusions in hematite

The Pb isotopic composition of the fluid inclusions follows the same pattern in the $^{206}Pb/^{204}Pb$ – $^{207}Pb/^{204}Pb$, $^{206}Pb/^{204}Pb$ – $^{208}Pb/^{204}Pb$, and $^{206}Pb/^{204}Pb$–$^{238}U/^{204}Pb$ diagrams (Fig. 7a–c). Most distinctly, the Pb isotopic composition of fluid inclusions is less radiogenic than that of the corresponding hematite hosts. Mineral–inclusion pairs define three types of pattern: (1) The $^{207}Pb/^{206}Pb$ slope is flat and could correspond to a Paleozoic event. This pattern is found in hematite from the Au-bearing *jacutinga*-style deposits at Gongo Soco and Itabira; (2) the $^{207}Pb/^{206}Pb$ slope is steep and may correspond to a Paleoproterozoic age. This pattern is found in the barren veins from Fábrica and Córrego do Feijão and possibly in the Au-bearing *jacutinga*-style veins at Gongo Soco (Fig. 7a); (3) The Pb isotopic composition of fluid inclusions and host-mineral is essentially identical. This relation is only observed in the barren veins from Fábrica. The relation among hematite samples from the Gongo Soco deposit is complicated, as the fluid inclusions fall on the flat trend of all other auriferous hematite veins (*jacutinga*), whereas the individual sample pairs (hematite host + fluid inclusion) fall on steep trends. This anomalous pattern may reflect that there was no common initial Pb isotopic composition in these samples. Instead, there may have been contributions of old hematite in the analyzed hematite fraction.

Gold

The Pb isotopic composition of gold samples from *jacutinga* veins at Gongo Soco align along the steep 2.7–1.9 Ga trend in the $^{206}Pb/^{204}Pb$ vs. $^{207}Pb/^{204}Pb$ diagram (Fig. 7a Table 4) with some samples being displaced to the right of this trend. Most gold samples have low Pb contents and very low U contents, which makes in situ Pb growth insignificant. The shift of the data to the right reflects in situ Pb growth. The alignment of the data, however, reflects a derivation of Pb from different sources. The Pb of the gold samples is distinctive by its higher $^{207}Pb/^{204}Pb$ and lower $^{208}Pb/^{204}Pb$ values (at comparable $^{206}Pb/^{204}Pb$) from the hematite samples (Fig 7a, b). This implies that the gold may have been derived from a different source than the iron. The barren deposit of Córrego do Feijão is in its $^{208}Pb/^{204}Pb$ signature closest to the itabirite from the Itabira district (Olivo et al. 1996), whereas the Au-bearing *jacutinga* veins have $^{208}Pb/^{204}Pb$ values that are closer to the signature of Au. The Pb isotopic signature of Au suggests its derivation from a source characterized by relatively low Th/U values such as Archean basement rocks or local itabirites (cf. Rudnick and Fountain 1995).

Metallogenic implications

Fluid evolution

Studies of fluid inclusions hosted in specular hematite from various occurrences in the QF have revealed that specular hematite from barren veins and Au–Pd–(Pt)-bearing *jacutinga*-style mineralization at Gongo Soco precipitated from fluids that show narrow ranges in salinity and homogenization temperatures. This may be due to similar formation conditions or fluid origin from common sources, although the veins from Fábrica and Córrego do Feijão are barren of Au, Pd, and Pt. Crush-leach analyses demonstrate Cl and SO_4 to be the major anions in the quartz- and hematite-forming fluids (Table 2). These results are in good agreement with previous studies of fluid inclusions in quartz from quartz–hematite veins in the Ouro Fino area (Boiron et al. 1999). Acid Cl–SO_4 waters are typical of geothermal systems but unusual for crustal fluids. The halogen ratios of fluid inclusions in quartz and hematite from all deposits are consistent with an initial halite-saturated fluid that gained extra Br (low Cl/Br ratios) by dissolving and reprecipitating halite, and was then subsequently diluted. The high sulfate concentrations of the analyzed fluids may also be derived by leaching of evaporites (gypsum). The narrow ranges of Na/K ratios, as well as elevated amounts of Ca and Li, in the analyzed fluids indicate water–rock interaction between the ore-forming fluids and granites and/or gneisses of the crystalline basement.

Jacutinga-style mineralization in the Itabira district, which is situated in the high-strain (high-metamorphic) domain (Fig. 1), is characterized by a similar fluid composition as the studied deposits in the low-strain domain, but experienced much higher temperatures (Fig. 4). Additionally, CO_2-rich fluids were trapped besides brines as fluid inclusions in hematite and quartz. Fluid inclusion petrography suggests contemporaneous trapping of both types of inclusions during crystal growth (Fig. 3e–g). Two scenarios are possible to explain the presence of the fluid inclusion assemblages in the studied samples: (1) unmixing of a single (supercritical) fluid, or (2) unmixing caused by a compositional change during fluid–rock interaction. Considering the high SO_4 content of the analysed fluid inclusions, the latter scenario implies that metamorphic fluids have reacted with evaporite-rich horizons during ascent.

In the first scenario, the observed fluid inclusion assemblages represent mixtures of two phases that formed when an originally homogeneous fluid reached the solvus during cooling or decompression (Diamond 1994). The hypothesis of trapping an immiscible fluid is supported by the consistency of the inclusion compositions with the location of tielines in the system H_2O–NaCl–CO_2 at a probable formation temperature of 320°C and pressure of 50 MPa (Fig. 8). The multiphase aqueous inclusions do not contain halite and their range in X(NaCl) is much smaller than the range in $X(CO_2)$ of

the coexisting carbonic aqueous inclusions (Fig. 8). Unmixing from a single, homogeneous parent fluid is also supported by the variation in the Cl/Br ratios at fairly constant Na/K ratios (Fig. 6). Mixing of two fluids of different composition, i.e. a hot carbonic fluid that mixed with a colder one, rich in sulfate, is rather unlikely because there is also an excellent correlation between the Na/Br and Cl/Br ratios (Fig. 5). Such a correlation should not be given in the case of mixing of at least two fluids, especially if the fluids had different temperatures. Therefore, it seems more likely that the fluids gained their salinity and sulfate content by dissolution of evaporites at greater depths prior to ascent.

Specular hematite from barren hematite–quartz veins in the low-strain domain as well as from *jacutinga*-style mineralization at Gongo Soco also precipitated from brines but does not contain any carbonic inclusions. However, the cation and anion ratios as well as the unusual high SO_4 content of the quartz and hematite-hosted fluid inclusions suggest a fluid origin from a similar source for all studied sites. The absence of CO_2 in hematite-hosted inclusions from veins in the low-strain domain may be attributed to carbonate precipitation or conversion of CO_2 to bicarbonate due to cooling during fluid migration from the high- to the low-strain domain. Such a model implies that the migration of fluids and formation of specular hematite in shear zones from all studied sites is related to a more or less contemporaneous event. If fluid migration occurred from deeper crustal levels to cooler, shallower levels westward, then the auriferous quartz–hematite veins of *jacutinga* style should be restricted to the eastern high-strain domain. In fact, the *jacutinga* veins have hithero been recognized in the eastern high-strain domain only, but they may also be present at greater depths in the western low-strain domain.

Origin of metals

The formation of specular hematite-rich veins at Itabira can be related to acid Cl–SO_4–CO_2 retrograde metamorphic fluids that interacted intensively with crystalline rocks. A Brasiliano age can be inferred from the $^{238}U/^{204}Pb$ vs. $^{206}Pb/^{204}Pb$ diagram (Fig. 7c) where specular hematite samples from the Itabira district and corresponding fluid inclusions fairly plot on or close to the reference line for 630 Ma.

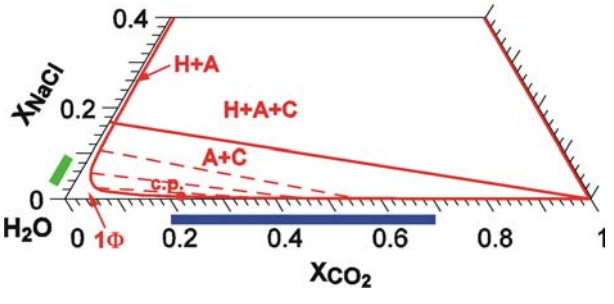

Fig. 8 Isobaric isothermal section in the system H_2O–CO_2–NaCl. *H* halite, *A* water-rich fluid, *C* CO_2-rich fluid, *c.p.* critical point; 1Φ = one phase field; solvus and tielines calculated using EOS of Duan et al. (1995); halite liquidus and critical point: Schmidt and Bodnar (2000). *Thick bars*: *green*—range in the salinity of multiphase aqueous inclusions in hematite from Itabira, *blue*—range in the estimated carbon dioxide concentrations of aqueous carbonic inclusions in hematite from Itabira

The least radiogenic Pb isotopic composition in the QF was measured on galena from orogenic gold deposits in the Archean Rio das Velhas Supergroup (Thorpe et al. 1984; $^{206}Pb/^{204}Pb$ = 13.626, $^{207}Pb/^{204}Pb$ = 14.598, $^{208}Pb/^{204}Pb$ = 33.301). Starting from such a composition and lasting until the Transamazonian orogeny, in situ Pb growth would evolve for different $^{238}U/^{204}Pb$ ($=\mu$) values to Pb isotopic compositions that fall on the red array as shown in Fig. 7. Samples with low μ values would have evolved less from their starting composition, whereas samples with high μ values would have evolved to more radiogenic compositions. There may be a lithologic control on the μ values, with higher values in more evolved felsic units than in mafic units. Depending on the source regions for the itabirite sequence in the Paleoproterozoic clastic-chemical sediments of the Minas Supergroup, different deposits may have constrasting Pb isotopic compositions. Undisturbed in-situ Pb growth in itabirites until the present would result in Pb isotopic compositions that fall between the 1.83 Ga reference line of Olivo et al. (1996) and the Archean-to Transamazonian Pb trend (Fig. 7). As the Pb isotopic composition of most samples falls to the right of the 1.83 Ga reference line, lead evolution towards highly radiogenic compositions occurred mainly after the Brasiliano orogeny (see also Fig. 7c). The scatter of the data in the $^{206}Pb/^{204}Pb$ vs. $^{238}U/^{204}Pb$ diagram either may reflect several events, most prominently a Brasiliano and a Transamazonian event (Fig. 7c), or highly radiogenic initial Pb isotopic compositions of some deposits at the time of the Brasiliano orogeny (dashed line in Fig. 7c). There is no reason to assume that no Pb evolution occurred in the source of the Pb incorporated in hematite of the *jacutinga* veins between the Transamazonian and the Brasiliano orogenies in the source of the Pb incorporated into hematite of the *jacutinga* veins. The relatively unradiogenic Pb isotopic composition of most of the hematite veins, as indicated by the intersection of the 630 Ma reference line with the $^{206}Pb/^{204}Pb$ axis in Fig. 7c, suggests that Pb in most hematite veins is derived from sources that had relatively low $^{238}U/^{204}Pb$ values. If the hematite veins in the Córrego do Feijão deposit formed during the Brasiliano orogeny, the source of the Pb in the hematite veins would have to have high $^{206}Pb/^{204}Pb$ values around 30–35 (Fig. 7c), which requires the Pb source of this deposit to have had higher $^{238}U/^{204}Pb$ values (ca. 45–60) than the other deposits.

The isotopic composition of trace Pb in palladian gold from Gongo Soco generally reflects lower $^{208}Pb/^{204}Pb$ values than the hematite samples from *jacutinga*-style veins from the same deposit. Furthermore, this trace Pb plots above the 1.83 Ga reference line and above the hematite field at either higher

Table 4 Pb isotope data of palladian gold from Gongo Soco, Brazil

Sample No.	Sample wt. [mg]	206Pb/204Pb	207Pb/204Pb	208Pb/204Pb	Conc. Pb [ppm]
GOS 1	389.66	21.278	16.425	35.893	88.40
GOS 3a	83.16	25.569	16.650	35.873	1.361
GOS 4	129.89	21.753	16.429	36.046	0.354
GOS 5	579.26	22.000	16.518	35.812	1.008
GOS 5r[a]	579.26	21.988	16.490	35.717	0.247
GOS 6-1	214.68	23.769	16.388	37.021	0.024
GOS 6-2	499.44	22.026	16.501	35.728	1.446
GOS 8	50.43	23.362	16.449	36.959	NA
GOS 8l[b]	—	20.263	16.063	37.051	—

NA not analyzed
[a]HCl leachate of sample GOS 8
[b]Replicate analysis of GOS 5

$^{207}Pb/^{204}Pb$ or lower $^{206}Pb/^{204}Pb$ (Fig. 7). The contrasting Pb isotopic composition between hematite and gold in the *jacutinga*-style veins possibly suggests that hematite incorporated significant amounts of locally derived material and that the veins may partly contain hematite grains originating from the older wall rock. The isotopic composition of trace Pb in gold is compatible with Archean source rocks characterized by high $^{238}U/^{204}Pb$ (μ) and relatively low $^{232}Th/^{204}Pb$ (κ) values. Possible source rocks with such properties could be granitoids and shales. Conversely, a derivation of the trace Pb in gold from the same source as the Pb in the itabirites or from the itabirite unit itself can be excluded (Fig. 7a). Considering the Archean felsic basement to be the source of the trace Pb in gold, these rocks could also be the source of U, which eventually gave rise to radiogenic Pb isotopic compositions in hematite and had controlling influence on the homogeneous Na/K ratios in hematite-hosted fluid inclusions. A felsic Archean basement, however, is unlikely to have provided Au and Pd. Instead, these two elements may be derived from the Archean supracrustal rocks that include voluminous units of mafic volcanic rocks (Guimarães 1970). For instance, metavolcanic and metapelitic rocks of the Nova Lima Group, which forms part of the Archean Rio das Velhas Supergroup, have Au contents of up to 20 ppb (Ribeiro-Rodrigues 1998). Itabirites are also known to have locally anomalous Au contents (20–330 ppb Au; cf. Ramanaidou et al. 1991; Klein and Ladeira 2000). Since Au and Pb do not have to originate from the same source, it is unclear whether the itabirites acted as source for the Au in the *jacutinga*-style veins or the enhanced Au contents in the itabirites were acquired from the fluids that formed the *jacutinga* veins. Since the Pb contents in felsic rocks are much higher than in mafic and ultramafic rocks, the Pb isotopic composition of a fluid that originated from the felsic basement and then percolated through mafic units may still be dominated by the felsic source. Thus, the fluid that transported Au and Pb into the *jacutinga* veins may have carried the Pb isotopic signature of source rocks distinct from the source of Au and Pd.

The formation of the *jacutinga*-style veins during the Brazilian orogenic cycle explains both the homogeneous nature of the fluids with respect to dissolved major components (e.g. Na/K, Cl/Br ratios and high SO_4 contents) and the heterogeneous character of the fluids with respect to CO_2 content and trace (Au, Pd, Pb, and U) constituents. Differences in proportions of major components are attributed to contrasting evolution histories of the fluid in terms of unmixing and cooling. In contrast, different contents in trace components probably reflect different depths of percolation in the basement which led to a spatially restricted distribution of Au–Pd–bearing *jacutinga*-style veins in the QF.

Conclusions

Specular hematite from auriferous (*jacutinga*) and barren veins in the QF was deposited from saline, SO_4-bearing brines of moderate to high temperatures. In the high-strain domain of the study area, CO_2-rich fluids were trapped besides brines as fluid inclusions in hematite and quartz probably due to unmixing of a single (supercritical) fluid. Halogen ratios as well as cation ratios suggest that the ore-forming fluids have leached evaporites and interacted with crystalline basement rocks.

The contrasting Pb isotopic characteristics of hematite and gold samples suggest different source lithologies for lead. A felsic basement is the likely source for trace Pb and U in gold from *jacutinga*-style mineralization at Gongo Soco but not the source for lead in hematite, which may contain significant contributions of Pb redistributed from the host itabirites. Similarly, different sources for Pb, Fe, Au, Pd, and Pt must be favored as Pb shows an isotopic composition indicative of old felsic crust, whereas Pd, Pt (and Au) rather originate from mafic rocks in the Archean basement. Considering a similar (Brasiliano) age for all studied hematite veins, the distribution of auriferous and barren hematite veins may reflect contrasting depths of fluid percolation during the Brasiliano orogeny.

Acknowledgements Part of this work was performed during a doctoral scholarship (A.R. Cabral) by *Deutscher Akademischer Austauschdienst* (DAAD). A.R.Cabral is grateful to *Companhia*

Vale do Rio Doce (CVRD) for fieldwork facilities and permission to sample, particularly to the mine geologists O.G. Rocha Filho, J.T. Rodrigues, H.F. Galbiatti, A.A.S. Gomes Jr. and A.V. Corrêa Neto. R.D. Jones is thanked for providing unpublished reports and maps of the Gongo Soco deposit and for discussions in the field. The attentive reviews by B. Lehmann and C.A. Rosière are gratefully acknowledged.

References

Alkmim FF, Marshak S (1998) Transamazonian orogeny in the Southern São Francisco craton region, Minas Gerais, Brazil: evidence for Paleoproterozoic collision and collapse in the Quadrilátero Ferrífero. Precamb Res 90:29–58

Banks DA, Giuliani G, Yardley BWD, Cheilletz A (2000) Emerald mineralisation in Colombia: fluid chemistry and the role of brine mixing. Mineral Deposita 35:699–713

Böhlke JK, Irwin JJ (1992) Laser microprobe analyses of Cl, B, I and K in fluid inclusions: implications for sources of salinity in some ancient hydrothermal fluids. Geochim Cosmochim Acta 56:203–225

Boiron M-C, Moisette A, Cathelineau M, Banks D, Monnin C, Dubessy J (1999) Detailed determination of paleofluid chemistry: an integrated study of sulphate-volatile rich brines and aquo-carbonic fluids in quartz veins from Ouro Fino (Brazil). Chem Geol 154:179–192

Cabral AR, Lehmann B, Kwitko R, Jones RD, Pires FRM, Rocha Filho OG, Innocentini MD (2001) Palladium-oxygenated compounds of the Gongo Soco mine, Quadrilátero Ferrífero, central Minas Gerais, Brazil. Mineral Mag 65:169–179

Cabral AR, Lehmann B, Kwitko R, Cravo Costa CH (2002a) The Serra Pelada Au–Pd–Pt deposit, Carajás mineral province, northern Brazil: reconnaissance mineralogy and chemistry of very high grade palladian gold mineralization. Econ Geol 97:1127–1138

Cabral AR, Lehmann B, Kwitko-Ribeiro R, Cravo Costa CH (2002b) Palladium and platinum minerals from the Serra Pelada Au–Pd–Pt deposit, Carajás mineral province, northern Brazil. Can Mineral 40:1451–1463

Cabral AR, Lehmann B, Kwitko R, Jones RD, Rocha Filho OG (2003a) On the association of palladium-bearing gold, hematite and gypsum in an *ouro preto* nugget. Can Mineral 41:473–478

Cabral AR, Rocha Filho OG, Jones RD (2003b) Hydrothermal origin of soft hematite ore in the Quadrilátero Ferrífero of Minas Gerais, Brazil: petrographic evidence from the Gongo Soco iron ore deposit. Appl Earth Sci (Trans Inst Min Metall B) 112:279–286

Chauvet A, Faure M, Dossin I, Charvet J (1994) A three-stage structural evolution of the Quadrilátero Ferrífero: consequences for the Neoproterozoic age and the formation of gold concentrations of the Ouro Preto area, Minas Gerais, Brazil. Precamb Res 68:139–167

Chauvet A, Piantone P, Barbanson L, Nehlig P, Pedroletti I (2001) Gold deposit formation during collapse tectonics: structural, mineralogical, geochronological, and fluid inclusion constraints in the Ouro Preto gold mines, Quadrilátero Ferrífero, Brazil. Econ Geol 96:25–48

Chemale F Jr (1987) Tektonische, lagerstättenkundliche und petrographische Untersuchungen im Eisenerzrevier Itabira, Minas Gerais, Brasilien. Clausthal-Zellerfeld, Clausthaler Geowissenschaftliche Dissertation, Technische Universität Clausthal, 140pp

Chemale F Jr, Quade H, Carbonari FS (1987) Economic and structural geology of the Itabira Iron District, Minas Gerais, Brazil. Z Geol Paläont I 1987:743–752

Chemale F Jr, Rosière CA, Endo I (1994) The tectonic evolution of the Quadrilátero Ferrífero, Minas Gerais, Brazil. Precamb Res 65:25–54

Clark AM, Criddle AJ, Fejer EE (1974) Palladium arsenide-antimonides from Itabira, Minas Gerais, Brazil. Mineral Mag 39:528–543

Davis RJ, Clark AM, Criddle AJ (1977) Palladseite, a new mineral from Itabira, Minas Gerais, Brazil. Mineral Mag 41:123

Diamond LW (1994) Introduction to phase relations of CO_2–H_2O fluid inclusions. In: De Vivo B, Frezotti ML (eds) Fluid inclusions in minerals: methods and application. Virginia Tech, Blacksburg, pp 131–158

Dorr JVN (1969) Physiographic, stratigraphic and structural development of the Quadrilátero Ferrífero, Minas Gerais, Brazil. US Geol Surv Prof Pap 641(A):110

Dorr JVN, Barbosa ALM (1963) Geology and ore deposits of the Itabira district, Minas Gerais, Brazil. US Geol Surv Prof Pap 341-C:110

Duan Z, Møller N, Weare JH (1995) Equation of state for the NaCl–H_2O–CO_2 system: Prediction of phase equilibria and volumetric properties.Geochim Cosmochim Acta 59:2869–2882

Gardner D (1826) In: Imperial Brazilian Mining Association—reports of the directors addressed to the share-holders, London, pp 128

Goldstein RH, Reynolds TJ (1994) Systematics of fluid inclusions in diagenetic minerals. SEPM Shourt Course 31:199

Guimarães D (1970) Arqueogênese do ouro na região central de Minas Gerais. Rio de Janeiro, Depart Nac Prod Mineral, Div Fom Prod Mineral, Bol 139:51

Hackspacher PC, Oliveira Jr VT, Siemes H, Rosière CA, Moreno MMT (2001) Textures of hematitic and itabiritic iron ores in the Conceição mine, Quadrilátero Ferrífero, Minas Gerais, Brazil. Z Dt Geol Ges 152:467–478

Harder EC, Chamberlin RT (1915) The geology of central Minas Geraes, Brazil. J Geol 23:341–378

Hart R (1827) In: Imperial Brazilian Mining Association—third report of the directors addressed to the share-holders, and an appendix: London, pp 75

Hartt CF (1870) Geology and physical geography of Brazil. Fields, Osgood, and Co., Boston, 620p

Hasui Y, Magalhães FS, Ramos JMS, Carbonari FS, Sandroni SS (1994) Modelo estrutural da mina de ferro do Cauê. Geociên 13:149–165

Henwood WJ (1871) On the gold mines of Minas Geraes in Brazil. Trans Roy Geol Soc Cornw 8:168–370

Hoefs J, Müller G, Schuster AK (1982) Polymetamorphic relations in iron ores from the Iron Quadrangle, Brazil: the correlation of oxygen isotope variations with deformation history. Contr Mineral Petrol 79:241–251

Hussak E (1904) Über das Vorkommen von Palladium und Platin in Brasilien. Sitzungsber math-naturwiss Kl Kaiserl Akad Wiss 113:379–468

Jedwab J, Cassedanne J (1998) Historical observations on oxygen-bearing compounds of platinum and palladium in Minas Gerais, Brazil. Can Mineral 36:887–893

Johnson PN, Lampadius WA (1837) Über brasilianisches Palladgold und dessen Ausbringen und Scheidung. J Prakt Chem 11:309–315

Klein C, Ladeira EA (2000) Geochemistry and petrology of some Proterozoic banded iron-formations of the Quadrilátero Ferrífero, Minas Gerais, Brazil. Econ Geol 95:405–428

Kwitko R, Cabral AR, Lehmann B, Laflamme JHG, Cabri LJ, Criddle AJ, Galbiatti HF (2002) Hongshiite (PtCu) from itabirite-hosted Au–Pd–Pt mineralization (jacutinga), Itabira district, Minas Gerais, Brazil. Can Mineral 40:711–723

Lobato LM, Ribeiro-Rodrigues LC, Zucchetti M, Noce CM, Baltazar OF, Silva LC, Pinto CP (2001) Brazil's premier gold province. Part I: the tectonic, magmatic, and structural setting of the Archean Rio da Velhas greenstone belt, Quadrilátero Ferrífero. Mineral Deposita 36:228–248

Lüders V (1996) Contribution of infrared microscopy to fluid inclusion studies in some opaque minerals (wolframite, stibnite, bournonite): metallogenetic implications. Econ Geol 91:1462–1468

Lüders V, Gutzmer J, Beukes NJ (1999) Fluid inclusion studies in cogenetic hematite, hausmannite, and gangue minerals from high-grade manganese ores in the Kalahari manganese field, South Africa. Econ Geol 94:589–596

Marshak S, Alkmim FF, Jordt-Evangelista H (1992) Proterozoic crustal extension and the generation of dome-and-keel structure in an Archaean granite-greenstone terrain. Nature 357:491–493

Meireles EM, Silva ARB (1988) Depósito de ouro de Serra Pelada, Marabá, Pará. In: Schobbenhaus C, Coelho CES (eds) Princ dep min do Brasil, vol III. Brasília, Depart Nac Prod Min, Comp Vale do Rio Doce, pp 547–557

Moine B, Sauvan P, Jarousse J (1981) Geochemistry of evaporite. bearing series: a tentative guide for the identification of meta-evaporites. Contrib Mineral Petrol 76:401–412

Moore SL (1969) Geology and ore deposits of Antônio dos Santos, Gongo Soco and Conceição do Rio Acima quadrangles, Minas Gerais, Brazil. US Geol Surv Prof Pap 341-I:48

Oliveira EP (1932) Genesis of the deposits of auriferous jacutinga. EconGeol 32:744–749

Olivo GR, Gauthier M (1995) Palladium minerals from the Cauê iron mine, Itabira district, Minas Gerais, Brazil. Mineral Mag 59:455–463

Olivo GR, Gauthier M, Bardoux M, Sá EL, Fonseca JTF, Carbonari F (1995) Palladium-bearing gold deposit hosted by Proterozoic Lake Superior-type iron-formation at the Cauê iron mine, Itabira district, southern São Francisco craton, Brazil: Geologic and structural controls. Econ Geol 90:118–134

Olivo GR, Gauthier M, Gariépy C, Carignan J (1996) Trans-amazonian tectonism and Au-Pd mineralization at the Cauê mine, Itabira district, Brazil: Pb isotopic evidence. J South Am Earth Sci 9:273–279

Olivo GR, Gauthier M, Williams-Jones AE, Levesque M (2001) The Au-Pd mineralization at the Conceição iron mine, Itabira district, southern São Francisco craton, Brazil: an example of a jacutinga-type deposit. Econ Geol 96:61–74

Pires FRM (1983) Greenstones as a part of the Minas Supergroup in the Quadrilátero Ferrífero, Minas Gerais, Brazil. Rev Bras Geol 13:106–112

Pires FRM (1995) Textural and mineralogical variations during metamorphism of the Proterozoic Itabira Iron Formation in the Quadrilátero Ferrífero, Minas Gerais, Brazil. An Acad Brasil Ciên 67:77–105

Pires FRM (2003) Distribution of hard hematite ore at the Quadrilátero Ferrífero, Minas Gerais, Brazil, and its possible genetic significance. Appl Earth Sci (Trans Inst Min Metall B) 112:31–37

Ramanaidou E, Cathelineau M, Dubessy J, Le Gleuher M (1991) Gold mobility during hydrothermal and supergene alteration of BIF (Itabirites), Ouro Fino syncline, Brazil. In: Ladeira EA (ed) Brazil Gold Balkema, Rotterdam, pp 91:729–733,

Roedder E (1984) Fluid Inclusions. Mineral Soc Am, Rev Mineral 12:643

Romer RL (2003) Alpha recoil in U–Pb geochronology: effective sample size matters. Contrib Mineral Petrol 145:481–491

Romer RL, Rocholl A (2004) Activity disequilibrium of ^{230} Th, ^{234}U, and ^{238}U in old stilbite: effects of young U mobility and α-recoil. Geochim Cosmochim Acta 68:4705–4719

Romer RL, Heinrich W, Schröder-Smeibidl B, Meixner A, Fischer C-O, Schulz C (2005) Elemental dispersion and stable isotope fractionation during reactive fluid-flow and fluid immiscibility in the Bufa del Diente aureole, NE-Mexico: evidence from radiographies and Li, B, Sr, Nd, and Pb isotope systematics. Contrib Mineral Petrol, (in press)

Rosière CA, Rios JR (2004) The origin of hematite in high-grade iron ores based on infrared microscopy and fluid inclusion studies: the example of the Conceição mine, Quadrilátero Ferrífero, Brazil. Econ Geol 99:611–624

Rosière CA, Siemes H, Quade H, Brokmeier H-G, Jansen EM (2001) Microstructures, textures and deformation mechanisms in hematite. J Struct Geol 23:1429–1440

Rudnick RL, Fountain DM (1995) Nature and composition of the continental crust: a lower crustal perspective. Rev Geophys 33:267–309

Schmidt C, Bodnar RJ (2000) Synthetic fluid inclusions XVI. PVTX properties in the system H_2O–NaCl–CO_2 at elevated temperatures, pressures and salinities. Geochim Cosmochim Acta 64:3853–3869

Scott HK (1902) The gold field of the state of Minas Gerais, Brazil. Trans Am Inst Min Eng 33:406–444

Shannon RD (1976) Revised effective ionic radii and systematic studies of interatomic distances in halides and chalcogenides. Acta Cryst 32:751–767

Thorpe RI, Cumming GL, Krstic D (1984) Lead isotope evidence regarding age of gold deposits in the Nova Lima district, Minas Gerais, Brazil. Rev Bras Geoc 14:147–152

Verma SP, Santoyo E (1997) New improved equations fpr Na/K, Na/Li and SiO_2 geothermometers by outlier detection and rejection. J Volcanol Geotherm Res 79:9–23

Varajão CAC, Colin F, Vieillard P, Melfi AJ, Nahon D (2000) Early weathering of palladium gold under lateritic conditions, Maquiné mine, Minas Gerais, Brazil. Appl Geochem 15:245–263

Wendt I, Carl C (1991) The statistical distribution of the mean squared weighted deviation. Chem Geol 86:275–285